Radiology Research Day 2026 Program

Department of Radiology

Duke University School of Medicine

The Department of Radiology is pleased to host the inaugural *Radiology Research Day*, a dedicated forum showcasing the scholarly work of students and trainees. This event aims to celebrate research advancements in radiologic science, spark innovation, and foster future collaborations.

Schedule of Events

All events will take place in The Great Hall of Trent Semans Center for Health Education (Level 0)

7:30-8:00 AM	**Podium Presentations**
8:00-9:00 AM	**Poster Presentations and Research Group Expo**
12:00-12:15 PM	**Presentation of Awards**
12:15 – 1:00 PM	**Networking Lunch (RSVP Required) and Speaker Panel** *"How Research Will Transform the Future of Radiology"* Joseph Lo PhD, Kyle Lafata PhD, Lars Grimm MD MHS, and Evan Calabrese MD PhD

Award Categories

Best Overall - Basic Science
Best Overall - Clinical or Education
Best Oral Presentation
Best Undergraduate Student Project
Best Medical Student Project
Best Graduate Student Project
Best Trainee (Resident, Fellow) Project

Special Thanks to:

Mustafa Bashir, MD

Evan Calabrese, MD PhD

Katherine Cheng, MD

Danielle Corrigan-Webster

Jen Eberhard

Debbie Griffin

Lars Grimm, MD MHS

Lisa Ho, MD

Connie Kim, MD

Jeanne Kirschner

Kyle Lafata, PhD

Eun Langman, MD

Joseph Lo, PhD

Jon Martin, MD

Charles Maxfield, MD

Derek Nguyen, MD

Erik Paulson, MD

Scott Robertson, PhD

Joshua Wilson, PhD

Oral Presentations

Perkons, N. "Intravascular Ultrasound-Guided Transcaval Cisterna Chyli Access for Lymphatic Intervention: A Proof-of-Concept Study in a Porcine Model"

Olivas, K. "A Quantitative Framework for Opportunistic Bone Health Screening Using Photon-Counting CT Localizer Radiographs"

Garcia-Alcoser, M. "Evaluating Large Language Models for Automated Annotation of CT Radiology Reports"

Srinivasan, S. "Longitudinal Evaluation of Muscle Stiffness and Comparison to Clinical Measurements Using Shear Wave Elasticity Imaging"

Poster Presentations

Alsaihati, N. "Generalized ontological framework for CT data profiling and characterization"

Cai, Y. "Feasibility of a Motion Artifact Assessment Algorithm in Chest CT Using Combined Virtual and Clinical Data"

Chari, T. "Impact of demographics on surveillance and survival in post-resection orthopedic Sarcoma patients"

Christensen, S. "Photon-Counting Detector vs. Energy-Integrating Detector CT Myelography for Detecting CSF-Venous Fistulas in Spontaneous Intracranial Hypotension: Lower Radiation Dose"

Costelle, A. "Standardized Mapping of 129Xe Chemical Shift Heterogeneity in Pulmonary Capillary Red Blood Cells as a Biomarker for Pulmonary Hypertension"

Dahal, L. "Organ-Aware Attention Improves CT Triage and Classification"

Du, K. "Same-Session Repeatability of Single-Breath Fractional Ventilation Measurements Derived from 129Xe Gas Exchange MRI"

Felice, N. "Development of a 3-dimensional, material-specific computational coronary artery plaque growth model for use in virtual imaging trials"

Fenwick, D. "Thermal modeling of an x-ray anode: a radiography case study"

Heirman C. "Evaluating quantitative imaging biomarkers of chemoradiation resistance in murine head and neck squamous cell carcinoma"

Ho, F. "Task-specific Evaluation of Photon-Counting CT Using a 3D-Printed Anthropomorphic Lung Phantom with COPD Pathology"

Huang, Z. "Optimizing GBRT Models to Predict Brain Toxicity in Multi-Target SRS: A Comparative Evaluation"

Kadi, D. "What is the risk of HCC in hypervascular LI-RADS 3 observations in routine clinical practice?"

Kelly, K. "Characterizing the Innate Immune Response to Chemoradiation in a Murine Model of Head and Neck Squamous Cell Carcinoma"

Lavergne, A. "CT-Based Body Composition in a Pilot Cohort of Lung Transplant Candidates"

Lee, S. "Improving the precision of hyperpolarized 129Xe MR spectroscopy using heart rate-based spectral averaging"

Li, X. "Computational characterization of lymphocyte topology on whole slide images of glomerular diseases"

McCabe, C. "Synthesizing heterogeneous lung lesions for virtual imaging trials"

Milki, N. "Balloon-expandable covered stent for malignant compression of the right pulmonary artery: a palliative case report"

Montero, I. "Disparities of access to medical imaging technology across the U.S. as a function of social vulnerability"

Montero, I. "Modeling the Radiology Department: A Digital Twin Approach"

Mosley, I. "Assessing Motion Artifacts in Ultra-High Resolution CT for Pancreatic Cancer Imaging"

Murphy, D. "Lymphocytic Feature Characterization Using a Deep Learning Algorithm on Post-Radiation Lymph Nodes"

Nadkarni, R. "A Virtual Preclinical Photon-Counting CT Framework for Truth-Based Imaging Optimization in Cancer Studies"

Nam, J. "Association of CT-Based Body Composition and Lipoprotein(a)"

Nasthas, A. "Bridging Anatomy and Radiology: The Educational Impact of CT Interpretation during Gross Anatomy in the First Year Medical School Curriculum"

Perkons, N. "EPIC Workflow Changes to Improve Interventional Radiology Consult Triage and Reduce Overnight Paging Volume"

Perkons, N. "Retrospective Review of Outcomes Following Apheresis Port Placement"

Reed, B. "Difference in Image Quality between Natively Reconstructed and PACS Reformatted CT Images"

Riley, B. "A Patient-Specific Digital Twin Framework to Model Spatial Immune Dynamics in Head and Neck Squamous Cell Carcinoma"

Stevens, J. "A stochastic modeling framework to integrate radiomic feature representations: development and proof of concept application to PET/CT images of oropharyngeal cancer"

Tan, R. "Investigating Intra-tumoral Heterogeneity Driven by Nutrient Dynamics Using an In-silico Avascular Tumour Growth Model"

Zaveri, S. "Scan-Rescan Repeatability of Hippocampal Volume Measurements in Patients with Low-grade Glioma: Comparison of Automated Software Packages"

Oral Presentations

Intravascular Ultrasound-Guided Transcaval Cisterna Chyli Access for Lymphatic Intervention: A Proof-of-Concept Study in a Porcine Model

First Author: Nicholas Perkons, MD
Mentor: Brendan Cline, MD
Training Level: Resident

A Quantitative Framework for Opportunistic Bone Health Screening Using Photon-Counting CT Localizer Radiographs

First Author: Katie Olivas, MS
Mentor: Ehsan Abadi, PhD, Ehsan Samei, PhD
Training Level: Medical Physics Graduate Program

Evaluating Large Language Models for Automated Annotation of CT Radiology Reports

First Author: Michael Garcia-Alcoser, MS
Mentor: Joseph Y. Lo, PhD
Training Level: Medical Physics Graduate Program

Longitudinal Evaluation of Muscle Stiffness and Comparison to Clinical Measurements Using Shear Wave Elasticity Imaging

First Author: Shruthi Srinivasan, BS
Mentor: Kathryn R. Nightingale, PhD
Training Level: BME PhD Candidate

Perkons, N. “Intravascular Ultrasound-Guided Transcaval Cisterna Chyli Access for Lymphatic Intervention: A Proof-of-Concept Study in a Porcine Model”

First Author: Nick Perkons, MD
Mentor: Brendan Cline, MD
Training Level: Resident
Location: Podium Presentation

Background: Lymphatic interventions are an emerging frontier for Interventional Radiology. However, obtaining central lymphatic access can be difficult, time-consuming and risks injury to critical structures.

Objective: This study was designed to test our hypothesis that intravascular ultrasound (IVUS)-guided transcaval central lymphatic cannulation is technically feasible, with the potential to reduce procedure time and associated risk.

Methods: Four female swine underwent transcaval central lymphatic cannulation. Animals were fed a high-fat diet preceding non-survival experimentation. We utilized a side-firing phased-array sectoral IVUS catheter (ViewFlex Xtra ICE; St. Jude, Saint Paul, MN) to visualize and perform direct lymphatic puncture using a 21-gauge echogenic tip needle, inserted through a transjugular intrahepatic portosystemic shunt kit deployed in the common femoral vein. The first cohort of two animals underwent nodal lymphangiography for fluoroscopic delineation of the lymphatic system followed by IVUS-guided central lymphatic access. The second cohort began with attempted de novo IVUS-guided access, though nodal lymphangiography was performed if unsuccessful. After cannulation, thoracic duct embolization (TDE) was performed using coils and/or glue.

Results: The TD was successfully cannulated via an IVUS-guided transcaval approach in all four animals. The first two animals demonstrated that the most capacious segments of the cisterna chyli was often too far from the cava for direct access, requiring access of the central lymphatics in close proximity to the inferior vena cava. In the second cohort, 1 (of 2) attempts to access the central lymphatics de novo was successful, which was achieved at a level similar to the two animals from cohort one. In the remaining experiment de novo access failed; subsequent nodal lymphangiography demonstrated variant lymphatic anatomy with a diminutive CC; IVUS-guided lymphatic cannulation was achieved in this case after nodal lymphangiography. At the conclusion of all experiments, TDE was performed successfully.

Conclusions and Clinical Impact: These data demonstrate that IVUS-guided central lymphatic access is technically feasible and provides adequate stability to perform TDE, while highlighting that de novo success is dependent upon lymphatic anatomy. This approach has the potential to reduce the time required to obtain central lymphatic access and associated risks.

Olivas, K. “A Quantitative Framework for Opportunistic Bone Health Screening Using Photon-Counting CT Localizer Radiographs”

First Author: Katie Olivas
Mentor: Ehsan Abadi, PhD; Ehsan Samei, PhD
Training Level: Medical Physics Graduate Program
Location: Podium Presentation

Background: Dual-energy X-ray absorptiometry (DEXA) is the clinical standard for assessing areal bone mineral density (aBMD), yet its limited use in routine imaging workflows delays early osteoporosis detection. Photon-counting CT (PCCT) localizer radiographs, acquired during standard CT exams, present a low dose, underutilized alternative for opportunistic aBMD assessment.

Objective: This study investigated the feasibility of using photon-counting CT (PCCT) localizer radiographs for opportunistic aBMD assessment and osteoporosis screening.

Methods: Physical phantom experiments were conducted to assess the accuracy and feasibility of PCCT localizer radiographs for quantitative aBMD estimation, using DEXA as the reference standard. A lumbar spine phantom was scanned on a clinical PCCT system and with DEXA to compare aBMD values and radiation dose. Virtual imaging trials were performed to evaluate the robustness of aBMD quantifications from PCCT localizer radiographs across varying imaging conditions and patient sizes. Simulated conditions included a range of tube currents (30–140 mAs), bone health conditions (normal, osteopenic, osteoporotic), and patient sizes (BMI 23.7 and 30). A projection-based material decomposition algorithm was used to generate hydroxyapatite and water maps from the simulated localizers, from which aBMD estimates were derived.

Results: In physical phantom experiments, PCCT localizer radiographs produced aBMD estimates that closely matched DEXA measurements, with percent differences across vertebrae ranging from −4.95% to 5.05%. Radiation dose from PCCT localizers was comparable to DEXA and substantially lower than conventional CT. In virtual imaging trials, aBMD accuracy remained stable across tube current settings, with fluctuations limited to ~0.02 g/cm^2. Average mean absolute error (MAE) across all mAs and vertebrae was 0.0417 g/cm^2 for normal bone, 0.0627 g/cm^2 for osteopenic bone, and 0.0751 g/cm^2 for osteoporotic bone. Patient size influenced aBMD quantification accuracy, with MAE rising from ~0.10 g/cm^2 at BMI 23.7 to ~0.22 g/cm^2 at BMI 30.

Conclusion: PCCT localizer radiographs enable accurate, low dose aBMD estimation, showing strong agreement with DEXA and consistent performance across imaging conditions and patient sizes.

Clinical Impact: The use of PCCT localizer radiographs for opportunistic bone health assessment could enable osteoporosis screening in routine CT exams, providing earlier detection of low bone density and reducing fracture related morbidity without additional imaging or radiation exposure.

Garcia-Alcoser, M. “Evaluating Large Language Models for Automated Annotation of CT Radiology Reports”

First Author: Michael Garcia-Alcoser
Mentor: Joseph Lo, PhD
Training Level: Medical Physics Graduate Program
Location: Podium Presentation

Background: Annotating radiology reports enables the development of datasets that can be used to train downstream A.I. models and support a range of clinical natural language processing (NLP) tasks. While earlier methods such as rule-based algorithms (RBA) and BERT-based classifiers have been widely applied, large language models (LLMs) now offer promising capabilities for large-scale, automated annotation. Previous studies have primarily examined the use of LLMs for annotating chest X-ray (CXR) reports. However, their performance in accurately annotating CT reports has not been thoroughly evaluated.

Objective: To investigate the capability of LLMs to accurately annotate CT radiology reports and compare their performance with conventional NLP methods.

Methods: In this retrospective study, 40,833 chest–abdomen–pelvis (CAP) CT reports from 29,540 patients were analyzed, including 1,789 manually annotated reports across three organ systems. External validation employed the CT-RATE dataset. Three open-weight LLMs were tested using zero-shot prompting, and performance was measured by Cohen’s kappa (κ) and micro/macro F1 scores.

Results: Across 12,197 Duke CAP reports from 8,854 patients, Llama-3.1 8B and Gemma-3 27B achieved the highest agreement (median $\kappa = 0.87$). In the manually annotated set, Gemma-3 27B obtained the highest macro-F1 (0.82), followed by Llama-3.1 8B (0.79), while the RBA underperformed (0.64). On the CT-RATE dataset (lungs/pleura labels only), Llama-3.1 8B performed best (0.91), with Gemma-3 27B close (0.89). Variability across models largely stemmed from differences in labeling conventions, especially for subjective findings such as atelectasis.

Conclusion: Lightweight LLMs outperform rule-based methods for CT report annotation and generalize effectively across organ systems using zero-shot prompting. However, binary labels alone cannot capture the full nuance of radiology report language. LLMs offer a flexible and efficient solution that aligns more closely with clinical judgment and user needs. Future work will focus on multi-agent integration of these LLMs and designing a refined labeling schema to better represent the nuanced medical language present in radiology reports.

Clinical Impact: Lightweight LLMs can streamline CT report annotation by reducing manual effort and promoting standardized datasets for AI development. Integrating these models into multi-agent frameworks may further enable real-time triage and radiologist-in-the-loop workflows, improving clinical efficiency and consistency.

Srinivasan, S. “Longitudinal Evaluation of Muscle Stiffness and Comparison to Clinical Measurements Using Shear Wave Elasticity Imaging”

First Author: Shruthi Srinivasan
Mentor: Kathryn R. Nightingale, PhD
Training Level: PhD Student
Location: Podium Presentation

Background: Existing methods for longitudinal monitoring of skeletal muscle health are either qualitative, invasive, or costly. Previous work has shown the promise of 3D-rotational shear wave elasticity imaging (3D-RSWEI) to noninvasively characterize the anisotropic and nonlinear elastic mechanical properties of skeletal muscle.

Objective: Herein we quantify the longitudinal consistency of SWEI-based metrics, such as shear modulus and nonlinear elasticity, in healthy vastus lateralis muscle. We also compare these metrics between healthy muscle and diseased muscle of muscular dystrophy patients.

Methods: 3D-RSWEI uses a linear-array rotating about its central axis (the SWEI push axis) while collecting 2D planar SWEI data in 5-degree rotational increments. From acquired SWEI data, shear modulus is quantified along and across the direction of the muscle fibers. In vivo data is collected in the vastus lateralis of healthy volunteers and neuromuscular patients from an ongoing study approved by the Duke Institutional Review Board. Participants lay supine while 3D-RSWEI measurements are collected in the quadriceps muscle under varying degrees of knee flexion. A nonlinear elasticity parameter (Beta-L) is quantified by estimating an exponential growth constant between measured shear modulus along-the-fibers and knee flexion angle.

Results: Data collected in healthy volunteers collected over 3 months shows consistency of Beta-L to within a 7.5 +/- 3.3% coefficient of variation, and shear modulus along and across-the-fibers to within 8.0 +/- 3.3% coefficient of variation. Average Beta-L values are 0.021 +/- 0.001 1/deg in healthy volunteers, and 0.033 +/- 0.005 1/deg in neuromuscular patients. Average values for shear modulus at a high degree of knee flexion are 7.3 +/- 1.0 kPa and 1.1 +/- 0.1 kPa along and across-the-fibers in healthy participants, and 9.2 +/- 3.4 and 1.1 +/- 0.5 along and across-the-fibers in patient participants.

Conclusion: Variability of SWEI-based metrics for mechanical characterization of skeletal muscle are consistent to within 10% COV in healthy volunteers over time. Additionally, there are initial stark differences between SWEI-based metrics in patients with muscular dystrophies versus healthy volunteers.

Clinical Impact: This work contributes to our overall goal to develop non-invasive, quantitative imaging biomarkers for longitudinal monitoring of skeletal muscle health using ultrasonic shear wave elasticity imaging.

Map of Great Hall Poster Locations

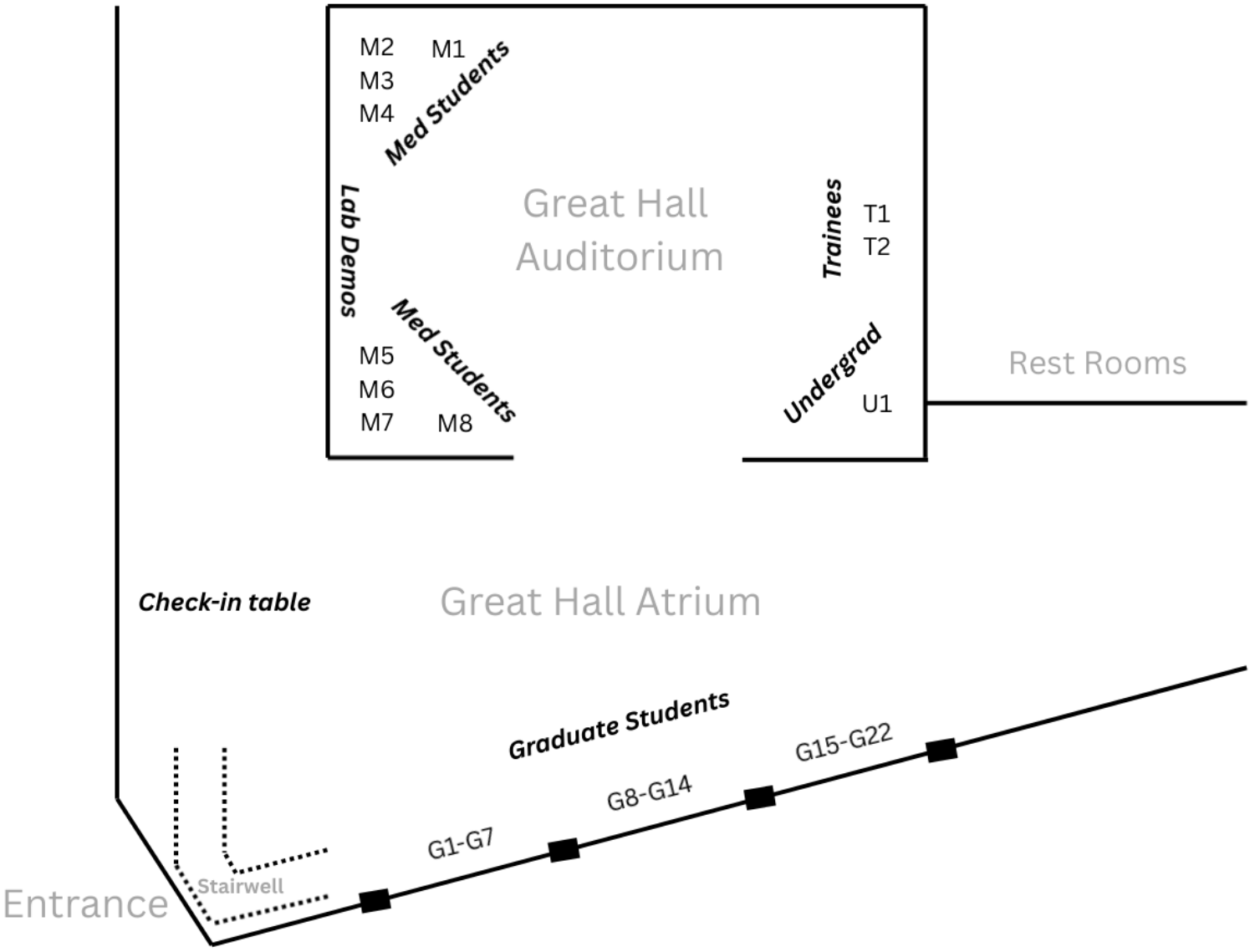

Poster Presentations

First Author	Mentor	Title	Location
Njood Alsaihati *Medical Physics Graduate Program*	Ehsan Samei, PhD	Generalized ontological framework for CT data profiling and characterization	G1
Yunrong Cai *PhD Student*	Ehsan Samei, PhD	Feasibility of a Motion Artifact Assessment Algorithm in Chest CT Using Combined Virtual and Clinical Data	G2
Tristan Chari *Medical Student*	Jon Martin, MD	Impact of demographics on surveillance and survival in post-resection orthopedic Sarcoma patients	M1
Soren Christensen *Medical Student*	Timothy J. Amrhein, MD	Photon-Counting Detector vs. Energy-Integrating Detector CT Myelography for Detecting CSF-Venous Fistulas in Spontaneous Intracranial Hypotension: Lower Radiation Dose	M2
Anna Costelle *Medical Physics Graduate Program*	Bastiaan Driehuys, PhD	Standardized Mapping of 129Xe Chemical Shift Heterogeneity in Pulmonary Capillary Red Blood Cells as a Biomarker for Pulmonary Hypertension	G3
Lavsen Dahal *PhD Student*	Joseph Lo, PhD	Organ-Aware Attention Improves CT Triage and Classification	G4
Kunyu (Kimi) Du *Undergraduate*	David Mummy, PhD	Same-Session Repeatability of Single-Breath Fractional Ventilation Measurements Derived from 129Xe Gas Exchange MRI	U1
Nicholas Felice *PhD Student*	Ehsan Abadi, PhD	Development of a 3-dimensional, material-specific computational coronary artery plaque growth model for use in virtual imaging trials	G5
David J. Fenwick, MS *Medical Physics Graduate Program*	Nicole Lafata, MS	Thermal modeling of an x-ray anode: a radiography case study	G6

Casey Claire Heirman *Medical Physics Graduate Program*	Kyle J. Lafata, PhD	Evaluating quantitative imaging biomarkers of chemoradiation resistance in murine head and neck squamous cell carcinoma	G7
Fong Chi Ho *PhD Student*	Ehsan Abadi, PhD	Task-specific Evaluation of Photon-Counting CT Using a 3D-Printed Anthropomorphic Lung Phantom with COPD Pathology	G8
Zhuoyun Huang (Murphy), MS *Medical Physics Graduate Program*	Chunhao Wang, PhD	Optimizing GBRT Models to Predict Brain Toxicity in Multi-Target SRS: A Comparative Evaluation	G9
Diana Kadi MD	Mustafa R. Bashir, MD	What is the risk of HCC in hypervascular LI-RADS 3 observations in routine clinical practice?	G10
Katelyn Kelly *PhD Student*	Kyle J. Lafata, PhD	Characterizing the Innate Immune Response to Chemoradiation in a Murine Model of Head and Neck Squamous Cell Carcinoma	G11
Alexa Lavergne *Medical Student*	Kirti Magudia, MD	CT-Based Body Composition in a Pilot Cohort of Lung Transplant Candidates	M3
Seth Lee *Medical Physics Graduate Program*	Bastiaan Driehuys, PhD	Improving the precision of hyperpolarized 129Xe MR spectroscopy using heart rate-based spectral averaging	G12
Xiang Li *PhD Student*	Kyle J. Lafata, PhD	Computational characterization of lymphocyte topology on whole slide images of glomerular diseases	G13
Cindy McCabe *PhD Student*	Ehsan Samei, PhD	Synthesizing heterogeneous lung lesions for virtual imaging trials	G14
Nubaira Milki *Medical Student*	Alex Solomon, MD	Balloon-expandable covered stent for malignant compression of the right pulmonary artery: a palliative case report	M4
Isabel Montero, MS	Ehsan Samei, PhD	Disparities of access to medical imaging technology across the U.S. as a function of social vulnerability	G15

PhD Student			
Isabel Montero, MS *PhD Student*	Ehsan Samei, PhD	Modeling the Radiology Department: A Digital Twin Approach	G16
Iman Ajani Mosley *Medical Student*	Ehsan Samei, PhD	Assessing Motion Artifacts in Ultra-High Resolution CT for Pancreatic Cancer Imaging	M5
Daniel Murphy, MS *Medical Physics Graduate Program*	Kyle J. Lafata, PhD	Lymphocytic Feature Characterization Using a Deep Learning Algorithm on Post-Radiation Lymph Nodes	G17
Rohan Nadkarni *PhD Student*	Cristian Tudorel Badea, PhD	A Virtual Preclinical Photon-Counting CT Framework for Truth-Based Imaging Optimization in Cancer Studies	G18
Jiung Nam *Medical Student*	Kirti Magudia, MD, PhD	Association of CT-Based Body Composition and Lipoprotein(a)	M6
Angelina Nasthas *Medical Student*	Eun Langman, MD	Bridging Anatomy and Radiology: The Educational Impact of CT Interpretation during Gross Anatomy in the First Year Medical School Curriculum	M7
Nick Perkons, MD *Resident*	Charles Kim, MD	EPIC Workflow Changes to Improve Interventional Radiology Consult Triage and Reduce Overnight Paging Volume	T1
Nick Perkons, MD *Resident*	Charles Kim, MD	Retrospective Review of Outcomes Following Apheresis Port Placement	T2
Beth Reed, MS *Medical Physics Graduate Program*	Justin Solomon, MD	Difference in Image Quality between Natively Reconstructed and PACS Reformatted CT Images	G19
Breylon Akeli Riley *Medical Physics Graduate Program*	Kyle J. Lafata, PhD	A Patient-Specific Digital Twin Framework to Model Spatial Immune Dynamics in Head and Neck Squamous Cell Carcinoma	G20

Jack B Stevens *PhD Student*	Kyle J. Lafata, PhD	A stochastic modeling framework to integrate radiomic feature representations: development and proof of concept application to PET/CT images of oropharyngeal cancer	G21
Runhe Tan *Medical Physics Graduate Program*	Kyle J. Lafata, PhD	Investigating Intra-tumoral Heterogeneity Driven by Nutrient Dynamics Using an In-silico Avascular Tumour Growth Model	G22
Suraj Zaveri *Medical Student*	Daniel Barboriak, MD	Scan-Rescan Repeatability of Hippocampal Volume Measurements in Patients with Low-grade Glioma: Comparison of Automated Software Packages	M8

Alsaihati, N. “Generalized ontological framework for CT data profiling and characterization”

First Author: Njood Alsaihati
Mentor: Ehsan Samei, PhD
Training Level: Medical Physics Graduate Program
Location: G1

Background: Inconsistent imaging procedure naming across and within institutions challenges clinical decision-making, quality assessment, and data analysis in radiology. For example, The American College of Radiology (ACR) CT Dose Index Registry (DIR) requires manual or semi-manual mapping of institutional study descriptions to RadLex Playbook IDs, a process prone to ambiguity and errors that impacts data consistency for analysis.

Objective: To develop a comprehensive data ontology framework and provide concrete demonstrations of its application for efficient CT data profiling and characterization.

Methods: A systematic review of existing literature and methodologies related to standardization in CT imaging informed framework development. The review identified key principles and gaps in nomenclature consistency and metadata standardization. The farmwork defines tags across study levels, irradiation events (scans), and series. These tags capture essential aspects of CT imaging workflows, including patient demographics, ordered and performed protocols, resulting interpretation, imaging environment, pharmaceutical usage, acquisition parameters, and reconstruction settings. Key examples were identified where the ontology framework offers practical benefits and impact.

Results: The data ontology framework was developed using generalizable tags, demonstrating its significant potential through two key areas. First, it enhances systems like the ACR CT DIR by reducing ambiguity in mapping and improving data consistency for benchmarking and quality assessment. Second, it addresses challenges associated with the Centers for Medicare & Medicaid Services (CMS) new quality measure, “Excessive Radiation Dose or Inadequate Image Quality for Diagnostic Computed Tomography (CT) in Adults.” By enabling efficient CT data profiling, the framework ensures data relevance, simplifies CT data complexity, and helps institutions maintain compliance while supporting clinically justified personalized care.

Conclusion: The data ontology framework addresses critical challenges in CT imaging, enabling targeted data analysis. Its applications highlight its potential to improve quality assessment, compliance, and data reliability in radiology.

Clinical Impact: The ontology facilitates large-scale data aggregation and targeted analysis for applications in clinical care, research, AI/ML, and quality improvement. It provides a foundation to quantify the net value of an imaging exam and articulate what is diagnostically gained from a procedure.

Cai, Y. “Feasibility of a Motion Artifact Assessment Algorithm in Chest CT Using Combined Virtual and Clinical Data”

First Author: Yunrong Cai
Mentor: Ehsan Samei, PhD
Training Level: PhD Student
Location: G2

Background: Motion artifacts in CT scans can degrade diagnostic image quality and are recognized as a critical factor that needs to be incorporated into quantitative imaging analysis. However, the requirement for extensive manual labeling remains a major barrier to developing deep learning–based approaches for artifact assessment.

Objective: To investigate the feasibility of a deep learning–based approach for motion artifact assessment in chest CT by training a model on combined virtual and clinical data.

Methods: A U-Net segmentation model was trained to localize motion artifacts using 99 respiratory-gated clinical CT series from patients and 44 motion-simulated CT series generated through a 4D XCAT–DukeSim framework. The trained network was evaluated on an independent 24 series pulmonary embolism dataset using multiple series-level aggregation metrics to indicate artifact severity.

Results: The model achieved reasonable series-level differentiation between motion-affected and motion-free scans, with the best-performing aggregation metric reaching an AUC of 0.89. Qualitative visualization revealed that the model correctly identified motion-affected regions in several cases, although false positives and false negatives were also observed.

Conclusion: The study demonstrates that combining virtual and clinical CT data enables effective deep learning–based motion artifact assessment and highlights the potential of hybrid training for artifact quantification.

Clinical Impact: This approach provides a scalable framework for automated CT image quality assessment, facilitating routine quality assurance and enabling integration of artifact evaluation into quantitative imaging workflows.

Chari, T. “Impact of demographics on surveillance and survival in post-resection orthopedic Sarcoma patients”

First Author: Tristan Chari
Mentor: Jon Martin, MD
Training Level: Medical Student
Location: M1

Background: Primary bone tumors (PBTs) are rare malignancies with high recurrence and poor survival rates, making timely post-surveillance imaging critical for early detection of metastasis and improved outcomes. While national guidelines recommend structured imaging protocols, adherence may vary across patient populations. Literature has demonstrated that imaging disparities exist among under-represented minorities (URMs), but little is known about these differences in the PBT patient population.

Objective: This study aims to evaluate the impact of race, socioeconomic deprivation, and insurance status on adherence to imaging surveillance within five years following the diagnosis and resection of sarcoma of the bone. It also examines how these factors relate to cancer-related mortality.

Methods: A retrospective cohort study evaluated the relationship between demographics and surveillance imaging adherence among PBT patients at a single institution. Out of 128 patients diagnosed with and surgically managed for a PBT between 2013 and 2018, 91 were chosen for analysis after excluding for metastatic disease at the time of resection and insufficient surveillance data. Surveillance data was collected from patients who were monitored for five years post-resection or until metastasis occurred, with adherence to surveillance imaging protocols and survival assessed over this period.

Results: The cohort comprised 91 patients (56% male, 44% female; 71% White, 24% Black or African American). Under-represented minority (URM) status was associated with 0.19 odds of receiving optimal imaging adherence (95% CI [0.05, 0.71], P = .01). Furthermore, URM patients had 3.20 odds of mortality compared to White patients during the five-year follow-up (95% CI [1.18, 8.67], P = .02).

Conclusion: At our institution, URM patients demonstrate significantly lower adherence to imaging surveillance and higher mortality rates following primary sarcoma resection.
Clinical Impact: These findings highlight the necessity for targeted interventions to address societal and health system factors that contribute to disparities in imaging adherence and survival among URM patients.

Christensen, S. “Photon-Counting Detector vs. Energy-Integrating Detector CT Myelography for Detecting CSF-Venous Fistulas in Spontaneous Intracranial Hypotension: Lower Radiation Dose”

First Author: Soren Christensen
Mentor: Timothy J Amrhein, MD
Training Level: Medical Student
Location: M2

Background: Spontaneous intracranial hypotension (SIH) is a debilitating condition caused by a spinal CSF leak or CSF venous fistula (CVF). CVFs are often difficult to detect, commonly requiring repeat, multi acquisition CT myelography (CTM), driving cumulative radiation exposure. Although photon-counting detector CT myelography (PCD CTM) improves CVF conspicuity versus energy integrating detector CT myelography (EID CTM), the radiation and cancer-risk consequences of choosing PCD versus EID remain unclear.

Objective: The primary objective was to compare exam level radiation dose for PCD CTM versus EID CTM in SIH. A secondary objective was to report modeled BEIR VII-based lifetime cancer risk.

Methods: This was a retrospective cohort study of consecutive patients meeting ICHD 3 criteria for SIH who underwent CTM for detecting causative CVF at a single institution from 3/2023–8/2025. For each exam, we recorded session dose length product (DLP, mGy·cm; sum across acquisitions), sex, and volume CT dose index (CTDIvol) of the exam’s most diagnostic series if applicable. Effective dose E (mSv) was estimated as $E = k \times DLP$ with $k = 0.015$ mSv/(mGy·cm) for thoracoabdominal coverage. Modeled lifetime attributable risk (LAR) for all solid cancers (incidence, mortality) was derived from BEIR VII sex specific 0.1 Gy coefficients. Group comparisons used Welch’s t tests.

Results: We analyzed 162 exams (42 PCD, 120 EID). Mean session DLP was considerably lower for PCD: 2101 mGy·cm for PCD and 6073 mGy·cm for EID, a 3972 mGy·cm difference corresponding to 65.4% reduction; $p<0.001$. In the CVF-positive subset (33 PCD, 103 EID), diagnostic-series CTDIvol was 7.6 vs 36.3 mGy, corresponding to 79.2% reduction; $p<0.001$. Secondary, model-based analyses showed lower BEIR VII LAR with PCD: all solid cancer incidence 0.34% vs 1.00% and mortality 0.17% vs 0.48% (PCD vs EID; both $p<0.001$).

Conclusion: The use of PCD in CT myelography for the detection of CVFs in SIH patients reduced session DLP by ~65% compared with EID CTM. In CVF-positive exams, diagnostic-series CTDIvol was ~79% lower. Together, these results show a substantially lower patient radiation burden with PCD. BEIR VII modeling indicated lower LAR with PCD. When available and clinically appropriate, PCD should be considered, especially for patients requiring repeat imaging.

Costelle, A. “Standardized Mapping of 129Xe Chemical Shift Heterogeneity in Pulmonary Capillary Red Blood Cells as a Biomarker for Pulmonary Hypertension”

First Author: Anna Costelle
Mentor: Bastiaan Driehuys, PhD
Training Level: Medical Physics Graduate Program
Location: G3

Background: Inhaled hyperpolarized 129Xe exhibits a unique chemical shift in pulmonary capillary red blood cells (RBCs). Its magnitude increases with blood oxygenation but decreases in patients with reduced capillary blood volume. Patients with pre-capillary pulmonary hypertension (PH) exhibit regions of elevated shift downstream of arteriolar occlusions. In these regions, capillary flow is slowed, lengthening transit time and paradoxically increasing RBC oxygenation. With preserved cardiac output, flow through the rest of the lung will increase, shortening transit times and reducing oxygenation. This heterogeneity can be mapped using 129Xe chemical shift imaging (CSI). However, quantifying these maps requires establishing a robust healthy reference distribution.

Objective: Establish an RBC CSI healthy reference distribution, and use thresholds derived from this distribution to quantify RBC shift heterogeneity in PH.

Methods: 129Xe CSI was acquired in healthy 18-30-year-old volunteers (N=11) and PH patients (N=6). Voxel-wise spectra were fit with Lorentzian RBC and gas-phase profiles, and a Voigt interstitial membrane profile. RBC shift maps were derived as the voxel-wise difference between the RBC and gas peak center frequencies. Maps from healthy volunteers were compiled into a single distribution. Thresholds from this distribution were used to calculate the percentage of defective, low, and high shift values in maps from all patients.

Results: The aggregate healthy reference distribution yielded a mean of 217.9ppm, with thresholds of -0.7/+0.8ppm (1 SD) and -1.4/+1.5ppm (2 SD). With these thresholds, healthy volunteers exhibited 3.2% defective, 15.9% low, and 4.6% high shift voxels. In contrast, PH patients exhibited 41.9% defective, 63.9% low, and 6.0% high shift.

Conclusion: In PH patients, elevated percentages of both low and high shift reflect significant heterogeneity driven by the redistribution of blood flow in the presence of pre-capillary occlusions. The particularly pronounced defective/low shift percentages may result from vascular remodeling like systemic-to-pulmonary artery collaterals.

Clinical Impact: 129Xe RBC CSI offers direct sensitivity to pulmonary vascular pathology. The dedicated CSI healthy reference distribution and functional thresholds enable more rigorous quantification of the heterogeneity observed in PH. Once optimized, this may permit non-invasive detection of localized arteriolar occlusions, facilitating more targeted application of highly invasive gold standard diagnostic methods.

Dahal, L. “Organ-Aware Attention Improves CT Triage and Classification”

First Author: Lavsen Dahal
Mentor: Joseph Lo, PhD
Training Level: PhD Student
Location: G4

Background: Study-level CT triage needs calibrated predictions and localized evidence. However, 3D anatomy, protocol shifts, and noisy report supervision often degrade off-the-shelf Vision Language Model (VLM) pipelines.

Objective: (1) Establish a transparent supervised baseline for CT triage with strong calibration. (2) Test whether organ-aware pooling and lightweight geometric/density cues further improve accuracy and interpretability across encoders and datasets.

Methods: We first train a rigorously tuned supervised GAP classifier on harmonized labels, apply per-label temperature scaling, and fix validation thresholds for reporting. Building on this, we propose ORACLE-CT: an encoder-agnostic, organ-aware head that attaches to either 2.5D token towers (eg, DINOv3, MedSigLIP) or native 3D trunks (Inflated ResNet-121, MedNeXt-3D, CT-Net). ORACLE-CT supports four aggregation modes: (i) Global Attention Pooling (GAP), (ii) global attention, (iii) organ-restricted attention with stable masked softmax, inside/outside priors, and an empty-mask fallback, and (iv) Organ-Scalar Fusion (OSF), which augments organ features with compact geometric/density scalars (e.g., volume, HU). We evaluate on CT-RATE with external testing on RAD-ChestCT, and on MERLIN (30 abdominal findings).

Results: The calibrated supervised GAP classifier sets a new state of the art versus reported linear-probe VLM baselines on CT-RATE and transfers better to RAD-ChestCT. On MERLIN, all supervised models exceed the released zero-shot baseline. Our best configuration—DINOv3 tokens with organ-aware pooling and OSF—achieves AUROC 0.83, AUPRC 0.64, F1 0.63, and balanced accuracy 0.72. Gains are largest for size- or density-driven targets (e.g., hepatomegaly/splenomegaly, prostatomegaly, pancreatic atrophy).

Conclusion: A carefully calibrated, supervised GAP baseline already outperforms linear-probe VLMs for CT triage. Adding organ-aware pooling and OSF yields further, interpretable improvements across both 2.5D and 3D encoders. ORACLE-CT sets a strong supervised reference for future CT-VLMs to surpass.

Clinical Impact: By coupling calibrated study-level predictions with organ-localized evidence, ORACLE-CT can prioritize urgent studies while providing interpretable cues that align with radiologists’ workflows.

Du, K. “Same-Session Repeatability of Single-Breath Fractional Ventilation Measurements Derived from 129Xe Gas Exchange MRI”

First Author: Kunyu (Kimi) Du
Mentor: David Mummy, PhD
Training Level: Undergraduate Student
Location: U1

Background: Hyperpolarized ^{129}Xe MRI provides a quantitative assessment of pulmonary ventilation. Traditional ventilation metrics such as ventilation defect percent (VDP) rely on relative intensity thresholds and have limited physiological interpretability. Fractional ventilation (FV) instead quantifies voxel-wise ventilation based on known inhaled xenon gas volume.

Objective: To extend FV analysis to gas-exchange ^{129}Xe MRI and evaluate its same-session repeatability relative to conventional 99th-percentile VDP (VDP-99).

Methods: 48 participants with idiopathic pulmonary fibrosis (IPF; age 71.8 ± 6.3 years) and 22 healthy volunteers (age 41.1 ± 14.9 years) underwent ^{129}Xe gas-exchange MRI with N4ITK bias correction. FV was computed as the xenon signal per voxel divided by the inhaled xenon volume, yielding voxel-wise fractional ventilation. Repeatability of mean FV was assessed with Bland–Altman analysis, intraclass correlation coefficient (ICC), and coefficient of repeatability (CR). VDP-FV was defined as voxels ≥ 2 SD below the healthy mean and compared with VDP-99 from conventional rescaling.

Results: Mean FV was 0.229 ± 0.047 in healthy subjects and 0.237 ± 0.071 in IPF ($p = 0.43$). Within-session repeatability for FV showed limits of repeatability (LoR) [−0.046, 0.056], ICC = 0.91, CR = 0.051. For VDP-FV, LoR = [−10.89, 7.75], ICC = 0.92, CR = 9.5, versus LoR = [−7.15, 7.6], ICC = 0.94, CR = 7.38 for VDP-99. When same-session scans were pooled, LoR between VDP-FV and VDP-99 were [−23.31, −19.83], ICC = 0.53, CR = 21.6.

Conclusion: FV analysis applied to ^{129}Xe gas-exchange MRI yields physiologically interpretable ventilation maps with strong within-session repeatability comparable to conventional methods.

Clinical Impact: This reproducible and quantitative framework for assessing regional fractional ventilation may enhance longitudinal monitoring and treatment-response evaluation in a range of lung diseases.

Felice, N. “Development of a 3-dimensional, material-specific computational coronary artery plaque growth model for use in virtual imaging trials”

First Author: Nicholas Felice
Mentor: Ehsan Abadi, PhD
Training Level: PhD Student
Location: G5

Background: Heart disease remains the leading cause of death in the United States, and accurate diagnosis is critical for effective treatment planning. Cardiac CT has become a key non-invasive tool for assessing coronary artery disease, providing direct visualization of arterial anatomy and plaque morphology. However, current CT-based evaluations face challenges including blooming and motion artifacts. Virtual imaging trials (VITs) have emerged as a cost-effective alternative to clinical trials for optimizing imaging technologies and protocols. For cardiac CT VITs to be clinically meaningful, realistic models of coronary artery plaques are required to accurately synthesize images across different modalities and acquisition parameters.

Objective: To develop a volumetric, material-specific plaque growth algorithm capable of generating physiologically informed coronary artery plaque models for use in VITs and demonstrate its utility in a pilot VIT.

Methods: A voxel-based plaque growth framework was developed to simulate the evolution of coronary artery plaques. The algorithm incorporates multiple materials, including foam cells, extracellular lipid pools, fibrous tissue, and calcifications, each following distinct, physiologically informed growth rules. Plaque growth occurs iteratively in three dimensions, enabling longitudinal and compositional variation along the vessel. A trained network predicts plaque morphology and material composition from input parameters, allowing user control over plaque severity and type. The resulting plaques were inserted into ten anthropomorphic virtual phantoms. Simulated CT scans were generated for each phantom using computational models of photon-counting CT (PCCT) and energy-integrating CT (EICT) scanners. Image quality was evaluated using root mean square error (RMSE) and structural similarity index (SSIM) metrics relative to the ground-truth phantoms.

Results: Simulated plaque growth followed physiological trends, including early lipid accumulation, fibrous cap formation, and progressive calcification. Assessment of generated plaques shows good agreement between predicted and output material composition and morphology. PCCT reconstructions yielded improved image quality and plaque conspicuity, achieving lower RMSE and higher SSIM values compared to EICT.

Conclusion: We present a novel model of coronary artery plaque growth that enables the generation of digital plaque volumes. This framework enhances the realism and diagnostic utility of cardiac CT VITs, facilitating future development and evaluation of emerging imaging technologies.

Fenwick, D. “Thermal modeling of an x-ray anode: a radiography case study”

First Author: David J. Fenwick, MS
Mentor: Nicole Lafata, MS
Training Level: Medical Physics Resident
Location: G6

Background: Multiple x-ray tube replacements at an off-site imaging center prompted concern that tube heating could be contributing to tube failure. The site frequently performs 5-view lumbar spine exams, often on patients with high body mass index, which requires multiple high mAs exposures. This study evaluates whether anode heat loading is a plausible contributor to tube damage.

Objective: Determine if anode heating is contributing to repeated tube failures at the Lincoln Community Health Center (LCHC) by collecting clinical exposure data and modeling anode heat deposition and cooling.

Methods: A two-week exposure timeline was constructed by linking patient attributes, image acquisition, and technique data. Patient attributes (accession number, height, weight) and image acquisition data (exposure date and time) were extracted from DICOM headers. Techniques (kV, mAs) were obtained from manual technique charts and technologist recorded techniques for automatic exposure control exams. For each exposure, anode heat deposition (kJ) was calculated, and the x-ray tube’s cooling curve was modeled using manufacturer specifications. Heating and cooling were simulated across the two-week period. Anode heat load was evaluated to determine whether it exceeded 90% of the maximum capacity (234 kJ). The exam with the highest calculated heat load was modeled to repeat 10 minutes later to simulate two high load exams back-to-back.

Results: The maximum heat load during the study period was 142 kJ. When a second high-load exam was simulated ten minutes after this peak, the heat load was 155 kJ. Across the ten-day evaluation period, anode heat exceeded 95 kJ on six days.

Conclusion: Anode heating may be a contributing factor to the increased frequency of x-ray tube replacements. Modeling a longer time interval and an assessment of repeat/reject rates, are warranted to further characterize anode heat loading. If anode heating is confirmed to play a significant role, protocol adjustments, including modification of techniques, exam selection, and potential implementation of patient weight limits, may be necessary in collaboration with radiologists.

Clinical Impact: X-ray tube replacements result in significant downtime and service costs. Protocol optimization may mitigate tube stress and support continued clinical use.

Heirman C. “Evaluating quantitative imaging biomarkers of chemoradiation resistance in murine head and neck squamous cell carcinoma”

First Author: Casey Claire Heirman
Mentor: Kyle J. Lafata, PhD
Training Level: Medical Physics Graduate Program
Location: G7

Objective: To evaluate the relationships between quantitative imaging biomarkers and chemoradiation resistance in head and neck squamous cell carcinoma (HNSCC) using preclinical mouse models.

Methods: Oral cavity tumors were generated in mice using three models with varied immunological profiles: (i) MOC1 (HPV-negative), (ii) MOC2 (HPV-negative), and (iii) MLM1 (HPV-positive) transplant tumors. Tumor dimensions were recorded three times per week, and chemoradiation therapy was initiated once tumors reached a volume of 50 mm^3. Treatment included cisplatin (5 mg/kg, intraperitoneally) and image-guided radiation therapy (8 Gy) administered on days 0 and 7. Tumor volume and SUVmax, normalized to mean liver uptake, were assessed on day 14 using 18F-FDG μPET/CT imaging. Radiomic features were derived from segmented tumor regions to assess metabolic texture, while pathomic features were extracted from digital pathology of necropsy specimens stained with H&E. Correlations between radiomic features, pathomic features, tumor immunological profiles, and overall survival (OS) were analyzed.

Results: MOC1 tumors displayed the highest radiosensitivity, with a median survival of 45 days, while MOC2 tumors (30 days) were the most resistant, and MLM1 tumors had a mixed response (39 days). Early response differences were significant ($p<0.0001$), with 26% of mice demonstrating tumor volume reduction by day 10. Multivariate Cox proportional hazard models with Bonferroni correction identified 31 significant radiomic features after adjusting for SUVmax. For instance, increased homogeneity in regions with low SUV uptake, characterized by Long Run Low Gray Level Emphasis, was associated with lower risk, suggesting connections to hypoxic or necrotic tumor regions. Tissue architecture were significantly different for responders and non-responders. Fusion of radiomic features with pathomic features resulted in a multiscale description of radiation resistance.

Conclusion: Preclinical mouse models are valuable for exploring chemoradiation resistance mechanisms and uncovering radiomic and pathomic patterns that reflect critical aspects of tumor biology.

Ho, F. “Task-specific Evaluation of Photon-Counting CT Using a 3D-Printed Anthropomorphic Lung Phantom with COPD Pathology”

First Author: Fong Chi Ho
Mentor: Ehsan Abadi, PhD
Training Level: PhD Student
Location: G8

Background: Photon-counting CT (PCCT) provides higher spatial resolution and improved noise performance compared with conventional CT, offering strong potential for quantitative assessment of chronic obstructive pulmonary disease (COPD). To fully utilize these advantages, imaging protocols must be optimized to balance resolution, noise, and dose for accurate biomarker quantification. However, multi-protocol patient studies are infeasible, and existing phantoms lack realistic COPD pathology, limiting systematic optimization.

Objective: This study aimed to establish a disease-specific, task-driven framework combining a realistic anthropomorphic COPD phantom and systematic PCCT protocol evaluation to identify configurations achieving accurate and reproducible biomarker quantification.

Methods: An anthropomorphic digital COPD phantom (110×140×70 mm^3; 0.2 mm voxel size) was created with anatomically realistic airways, vessels, emphysematous parenchyma, mucus plugs, and nodules. The model was fabricated using PixelPrint, a voxel-based 3D printing technique that reproduces CT attenuation and partial-volume effects. The phantom was scanned on a Canon PCCT prototype in Normal-Resolution (NR: 0.49×0.49×0.62 mm) and Super-High-Resolution (SHR: 0.24×0.24×0.21 mm) modes at CTDIvol levels of 5, 10, and 15 mGy. All data were reconstructed using Adaptive Iterative Dose Reduction (AIDR) with three kernel strengths. Quantitative evaluation included Global Noise Index (GNI), mean lung density (MLD), low-attenuation area below –950 HU (LAA-950), fifteenth percentile (Perc15), airway wall thickness (WT), wall area percentage (WA%), and mucus and nodule volume errors relative to ground truth. All analyses used fixed segmentation parameters for consistent cross-setting comparison.

Results: The SHR mode with stronger reconstruction consistently yielded the lowest noise, reduced parenchymal bias, and sharper boundaries than NR. GNI decreased with kernel strength, reaching its minimum in SHR-Strong settings. Parenchymal metrics approached ground truth, with mean LAA-950 error near zero and MLD bias below –2.5 HU. Airway accuracy improved with both resolution and strength, reaching WT error of 0.41±0.46 mm and WA% error of 3.82±7.48%. Mucus and nodule volumes remained stable across doses, with missed mucus volumes below 0.5 mm^3. SHR demonstrated superior spatial fidelity and quantitative reproducibility across all biomarkers.

Conclusion: The developed 3D-printed COPD phantom enabled comprehensive evaluation of PCCT, demonstrating that SHR combined with stronger iterative reconstruction provides optimal quantitative accuracy for airway, mucus, and parenchymal biomarkers.

Huang, Z. "Optimizing GBRT Models to Predict Brain Toxicity in Multi-Target SRS: A Comparative Evaluation"

First Author: Zhuoyun Huang (Murphy), MS
Mentor: Chunhao Wang, PhD
Training Level: Medical Physics Graduate Program
Location: G9

Background: Accurate prediction of radiation-induced brain toxicity remains a major challenge in stereotactic radiosurgery (SRS) for patients with multiple brain metastases. As the number and proximity of lesions increase, the risk of dose overlap and unintentional normal tissue exposure also rises. Reliable prediction of toxicity metrics such as V50%, V60%, and V66.7% is therefore essential for safe treatment planning. Machine learning models, including gradient boosted regression trees (GBRT), have shown promise in capturing nonlinear relationships between clinical and geometric variables, but their performance in multi-target SRS settings requires further evaluation.

Objective: This study aimed to develop and compare GBRT models for predicting V50%, V60%, and V66.7% brain toxicity metrics across multiple targets. A secondary aim was to determine whether incorporating unsupervised tumor clustering could improve model generalizability and prediction consistency.

Methods: Clinical and dosimetric data from 181 patients treated with single-isocenter multi-target SRS were analyzed. Each patient record included lesion number, total target volume, individual lesion volumes, and inter-lesion surface distances. Four GBRT configurations were trained: (1) a multi-output "3-in-1" model predicting all toxicity endpoints simultaneously; (2) a "3-in-1 Clustered" variant incorporating K-means–derived tumor clusters (k=3); (3) individual models trained separately for each endpoint; and (4) individual clustered models using the same clustering framework. Model performance was evaluated using 10-fold cross-validation, with mean absolute error (MAE), mean absolute percentage error (MAPE), R-squared (R^2), and uncertainty coverage as primary metrics.

Results: The multi-output 3-in-1 model achieved the lowest MAE (6.12 cc) and MAPE (20.83%) and the highest R^2 (0.88) across endpoints. Residual analysis demonstrated narrower error distributions for the clustered 3-in-1 model, particularly for V50% and V66.7%. Feature importance analysis consistently identified total brain volume as the most influential predictor.

Conclusion: A unified GBRT approach improved overall predictive accuracy compared with separate single-output models. Incorporating clustering modestly reduced variance without significantly altering mean prediction performance.

Clinical Impact: Integrating multi-output GBRT modeling provides a transparent, data-driven framework for assessing dose–volume toxicity relationships in multi-target SRS. This approach supports personalized treatment planning by improving the reliability of normal tissue toxicity predictions.

Kadi, D. “What is the risk of HCC in hypervascular LI-RADS 3 observations in routine clinical practice?”

First Author: Diana Kadi
Mentor: Mustafa R. Bashir, MD
Training Level: N/A
Location: G10

Background: The Liver Imaging Reporting and Data System (LI-RADS) categorizes liver observations based on their risk for HCC, with LI-RADS -3 observations (LR-3s) having an intermediate probability. Studies have shown that approximately one-third of LR-3 observations develop into hepatocellular carcinoma (HCC), however, this is not observed in clinical practice.

Objective: This study aimed to assess the HCC rate for hypervascular LR-3s.
Methods: We retrospectively identified consecutive MRI reports from 2013-2018 with hypervascular LR-3s in our institutional cohort. Observations with arterial phase hyperenhancement, no additional major/ancillary features, and <2 cm in size were included. Development of HCC was determined based on a composite reference standard.

Results: 129 patients (mean age 60+/-11 years, 69 [53.5%] male) with 166 LR-3s observations were included. Nine (8%, 95% CI [2.1-13.5%])) observations developed into HCC defined as change in category to LR-5 and exhibiting threshold growth in a median of 390 days (range 90-947) after index MRI. HCC rate for LR-3 was 2.4% at 1 year (95% CI [0-5.3%]).

Conclusion: We found a significantly lower rate of HCC development in LR-3s at 1 year compared to the literature. This could be due to underlying biases in the literature, for example requiring histologic confirmation of observations which could exclude many low risk LR-3s from analysis and falsely elevate the observed HCC rate.

Clinical impact: Our findings provide important insights into the management of patients with LR-3 observations. The low observed HCC rate suggests that not all LR-3s warrant aggressive follow- up or intervention.

Kelly, K. “Characterizing the Innate Immune Response to Chemoradiation in a Murine Model of Head and Neck Squamous Cell Carcinoma”

First Author: Katelyn Kelly
Mentor: Kyle J. Lafata, PhD
Training Level: PhD Student
Location: G11

Background: Immunotherapy remains an inefficient treatment modality for head and neck squamous cell carcinoma (HNSCC). Therefore, the aim of this study was to investigate the innate immune response to treatment and to elucidate the connection between innate and adaptive immunity.

Methods: We employed the murine oral squamous cell carcinoma (MOC2) model, which is HPV-negative, poorly immunogenic, and exhibits aggressive growth with metastatic potential. MOC2 cells were cultured in vitro and then inoculated (30,000 cells) into the buccal mucosa of ± Ccr2 C57BL/6 mice aged 6–11 weeks. When tumors reached approximately 35 mm^3 in volume, the mice were treated with combined chemoradiation consisting of an 8 Gy single-fraction radiotherapy and cisplatin (5 mg/kg, 30-minute uptake). Mice were then sacrificed at timepoints of 1, 3, and 7 days post-treatment for analysis of immune responses. Tumors, draining lymph nodes, and spleens were collected to assess the immune response to chemoradiation. Digital pathology and pathomic analysis of the tissues, along with bulk RNA sequencing of tumors, were conducted to characterize innate immune activity and associated transcriptomic changes.

Future Work/ impact: Animal radiobiological experiments provide a foundational understanding of treatment responses that can inform and improve human clinical therapies. Digital pathology enables spatial characterization of immune cell distribution within the tumor microenvironment over time. Complementary RNA sequencing provides insight into the molecular pathways and gene expression changes underlying the immune response, offering a deeper understanding of how the tumor adapts and immunologically reacts to chemoradiation. We will also extend this study to two additional murine tumor models, MOC1 (HPV-negative) and MLM1 (HPV-positive), which are less aggressive, and more immunogenic, to compare immune responses and assess how tumor phenotype influences the effects of chemoradiation.

Lavergne, A. "CT-Based Body Composition in a Pilot Cohort of Lung Transplant Candidates"

First Author: Alexa Lavergne
Mentor: Kirti Magudia, MD
Training Level: Medical Student
Location: M3

Background: Though lung transplantation is a life-saving treatment for end-stage lung disease, selecting candidates who will have optimal postoperative outcomes remains challenging. Body mass index (BMI) is commonly used to assess nutritional status and transplant eligibility, with both underweight (BMI < 18.5 kg/m^2) and class II-III obesity (BMI > 35 kg/m^2) associated with poorer outcomes. However, BMI does not capture underlying body composition, including proportions of muscle and adipose mass, or reflect the distribution of adipose tissue. CT-based body composition analysis allows precise quantification of skeletal muscle, visceral fat, and subcutaneous fat. Excess adiposity of the abdomen can impair respiratory mechanics and heighten systemic inflammation, potentially affecting transplant graft function. By capturing these nuanced differences, CT-based body composition offers a more accurate assessment of physiological reserves and refined risk stratification in the lung transplantation population.

Methods: We retrospectively analyzed a pilot cohort of 109 patients who underwent lung transplant evaluation with abdominal CT imaging at Duke University between 2019-2024. CT scans were analyzed using an automated deep learning workflow to quantify skeletal muscle, visceral fat, and subcutaneous fat at the L3 level. Wilcoxon rank sum test and Fisher's exact test were used to compare patients approved versus denied for lung transplantation. ANOVA with Tukey post-hoc tests were performed to compare tissue areas across BMI categories (<18.5: underweight, 18.5-24.9: normal, 25-29.9: overweight, ≥30: obese).

Results: This cohort included 66 patients approved for lung transplant and 43 patients denied, with no significant differences observed in age, race, or native lung disease between both groups. CT-based body composition demonstrated substantial heterogeneity within BMI categories. All three tissue areas were strongly associated with BMI (visceral fat, subcutaneous fat, and muscle; $p < 0.001$). Visceral fat and muscle area increased from underweight to overweight groups, but appeared to plateau at higher BMI, with no significant difference found between overweight and obese groups. In contrast, subcutaneous fat increased significantly across increasing BMI categories, with all pairwise comparisons significant ($p < 0.001$) except between underweight and normal BMI patients.

Conclusion: CT-based body composition varies markedly across BMI groups and reveals substantial metabolic heterogeneity in lung transplant candidates. While visceral fat and muscle area plateau at higher BMI groups in our cohort, subcutaneous fat area continues to increase, highlighting limitations of BMI as a stand-alone metric. Understanding these differences in CT-based body composition may improve risk stratification and guide lung transplant selection.

Lee, S. "Improving the precision of hyperpolarized 129Xe MR spectroscopy using heart rate-based spectral averaging"

First Author: Seth Lee
Mentor: Bastiaan Driehuys, PhD
Training Level: Medical Physics Graduate Program
Location: G12

Background: Traditionally, pulmonary MRI is challenging as the lungs produce low signal and create artifacts at tissue-air interfaces. This requires the use of specialized imaging sequences to maximize signal and image quality; however, one effective alternative is imaging using hyperpolarized gas contrast agents. Of these, 129Xe is particularly useful as it is soluble in the lung interstitium (membrane) and red blood cells (RBCs), allowing for direct visualization of pulmonary gas exchange. Reconstruction of gas exchange images requires knowledge of the RBC to membrane signal ratio (RBC:M), which is derived from MR spectroscopy. Most spectroscopy methods average a fixed number of spectra together to increase SNR; however, the RBC signal oscillates at the heart rate. This can affect the precision of RBC:M measurements.

Objective: Determine how cardiogenic RBC signal oscillations affect RBC:M measurements and improve repeatability by averaging spectra over complete cardiac cycles.

Methods: 129Xe MR spectroscopy was performed on a cohort of patients with idiopathic pulmonary fibrosis (N = 39) and healthy volunteers (N = 15). Theoretical variations in RBC:M measurements were derived analytically and compared to in vivo measurements. Repeatability of RBC:M measurements was assessed using the coefficient of repeatability (CR) for various averaging windows: 1 spectrum, 10 spectra, 1 second (67 spectra), and 1 cardiac cycle (~50 – 80 spectra).

Results: Effects of cardiogenic RBC signal oscillations on RBC:M measurements were found to be minimized at integer fractions of the cardiac cycle period. Repeatability was lower when averaging 1 spectrum (CR = 0.078) and 10 spectra (CR = 0.076) compared to 1 second (CR = 0.066) and 1 cardiac cycle (CR = 0.065).

Conclusion: Cardiogenic RBC signal oscillations introduce additional noise into RBC:M measurements, degrading precision. This noise can be minimized by averaging spectra over whole cardiac cycles. Similar repeatability can be achieved by averaging 1 second of data, likely because this matches a typical cardiac cycle period.

Clinical Impact: 129Xe gas exchange imaging provides valuable insights into a patient's pulmonary function. Image reconstruction is directly affected by the RBC:M value derived from spectroscopy; thus, precise measurement of RBC:M ensures consistent, reliable information is being produced by images.

Li, X. “Computational characterization of lymphocyte topology on whole slide images of glomerular diseases”

First Author: Xiang Li
Mentor: Kyle J. Lafata, PhD
Training Level: PhD Student
Location: G13

Background: The heterogeneous distribution of inflammation in the kidney is not well captured by conventional visual assessment. This study computationally quantified the topology of lymphocytic inflammation and tested its clinical relevance.

Objective: To develop and validate graph-based computational methods for quantifying lymphocytic inflammation topology and assess its association with disease progression in focal segmental glomerulosclerosis (FSGS) and Minimal Change Disease (MCD).

Methods: This study included 333 Hematoxylin & Eosin-stained whole slide images from two multi-institution collaborative databases: NEPTUNE/CureGN participants (155 FSGS, 178 MCD). Deep learning models were developed for automated segmentation of renal cortex and lymphocytes. Graph modeling was applied to all whole slide images, with nodes defined as lymphocytes and edges as spatial connections between neighbor lymphocytes. A graph-based habitat clustering algorithm identified dense versus sparse lymphocytic habitats. 26 quantitative pathomic features were extracted, capturing cell density, connectivity, clustering, and centrality. Association with disease progression (40% eGFR decline or kidney replacement therapy) was assessed using LASSO-regularized Cox proportional hazards models, adjusting for clinical and demographic characteristics. Two validation strategies were implemented: training on NEPTUNE with external validation on CureGN data, and 80/20 data partition of combined datasets.

Results: Multivariable Cox models integrating clinical/demographic variables with graph features achieved validation concordance indices of 0.736±0.072 in CureGN external validation and 0.757±0.071 in combined validation datasets. Average degree feature (overall connectivity) in dense habitats and k-core feature (clustering pattern strength) in sparse habitats showed significant associations with disease progression outcomes.

Conclusion: Topological characterization of lymphocytic inflammation identifies distinct immune habitats that provide complementary prognostic information beyond conventional assessment. These graph-based pathomic signatures represent potential digital biomarkers for disease progression prediction.

Clinical Impact: Implementation of these computational topology signatures could enhance risk stratification in FSGS/MCD patients, enabling personalized treatment strategies and improved patient management through objective, quantitative assessment of inflammatory patterns.

McCabe, C. “Synthesizing heterogeneous lung lesions for virtual imaging trials”

First Author: Cindy McCabe
Mentor: Ehsan Samei, PhF
Training Level: PhD Student
Location: G14

Background: Virtual imaging trials of malignancies require realistic models of lesions.

Objective: The purpose of this study was to create hybrid lesion models and associated tool incorporating morphological and textural realism.

Methods: The developed tool creates a lesion morphology based on input parameters describing its shape and spiculation. Internal heterogeneity is added as 3D clustered lumpy background (CLB), allowing for various types of lesions including full solid, semi-solid, and ground-glass lesions. To insert a lesion into a full body human model (e.g., XCAT phantom), the surrounding area is deformed and the edges of the lesion are blended into the surrounding background using a parameterizable Gaussian blurring technique. The developed lesion tool allows users to define lesion sizes either manually or automatically following population distribution of lesion sizes. The utility of the developed lesion tool was demonstrated by modeling both homogeneous and heterogeneous lung lesions and inserting them into human models (XCAT). The human models were imaged using a validated CT simulator (DukeSim). Images of heterogeneous lesions were visually comparable to clinical images. The radiomics features (58 features) were extracted from all image series. The most impactful parameter on feature values was the lesion type (full solid, semi-solid, or ground-glass). The two lesion generation techniques for full solid lesions (homogeneous vs. heterogeneous) was observed to have 9 of 58 features capture the structural differences between the two models.

Conclusion: The lesion tool proved capable to form different lung lesion types (full-solid, semi-solid, and ground-glass) through its input parameters to emulate the lesion characteristics of interest for a virtual lesion study.

Milki, N. “Balloon-expandable covered stent for malignant compression of the right pulmonary artery: a palliative case report”

First Author: Nubaira Milki
Mentor: Alex Solomon, MD
Training Level: Medical Student
Location: M4

Background: Compression of the pulmonary artery (PA) is a potentially fatal complication of advanced thoracic or metastatic malignancies. In cases of symptomatic malignant compression or prior radiation fibrosis, endovascular PA stenting offers immediate flow restoration and symptomatic improvement. The use of bare-metal stents in malignant PA compression has been described in prior case studies; however, their long-term efficacy is potentially limited by tumor ingrowth, restenosis, and vessel fragility in irradiated fields. Balloon expandable covered stents offer a viable alternative and potentially a more durable and safer treatment option.

Objective: Demonstrate a novel endovascular intervention that should be considered in multidisciplinary oncologic care.

Methods: Clinical information and imaging studies were retrospectively obtained from the electronic medical record of the patient treated at Duke University Hospital.

Results: Post-stenting completion arteriogram demonstrated significantly improved flow through the artery with a decrease in peak systolic PA pressure of 20 mmHg. No immediate complications were noted. Post-procedure echocardiography showed improved right ventricular size, a reduction in right ventricular systolic pressure from 109 mmHg to 56 mmHg, and preserved left ventricular function. A six-week follow-up CT angiogram showed stent patency without migration. The patient reported markedly improved exertional capacity. Conclusion: This case highlights the use of balloon expandable covered stents in providing durable symptomatic relief and hemodynamic improvement in patients with malignant PA stenosis at high risk for tumor in-growth and vessel fragility. In this patient, prior mediastinal radiation therapy and recurrent malignant vessel encasement after treatment prompted consideration of a covered rather than bare-metal stent, as the graft covering provided a barrier to tumor invasion and added a margin of safety against vessel injury.

Clinical Impact: Endovascular intervention represents an important and underutilized palliative treatment for malignant compression of the central pulmonary arteries, particularly when traditional treatment is contraindicated. Current literature in this area is limited to the use of bare-metal stents. In studies of malignant superior vena cava obstruction, recurrence after initial bare-metal stenting occurs in up to 41% of patients, often due to tumor in-growth. Covered stents, in contrast, have demonstrated higher long-term patency and lower stent occlusion rates and we demonstrate that they can be safely deployed in the pulmonary arteries.

Montero, I. “Disparities of access to medical imaging technology across the U.S. as a function of social vulnerability”

First Author: Isabel Montero
Mentor: Ehsan Samei, PhD
Training Level: PhD Student
Location: G15

Background: Equity of technological access and its impact on patient-centered care is an often- overlooked aspect of the clinical imaging landscape.

Objective: This study investigates the relationship between the age of CT scanners across the United States and the Social Vulnerability Index (SVI). The aim is to identify metrics that may indicate disparities in access to medical imaging technologies.

Methods: Data were extracted regarding the location and year of assembly of CT scanners across the U.S. from the Food and Drug Administration (FDA). SVI scores were sourced for each applicable U.S. County from the CDC-ATSDR (Center for Disease Control - Agency for Toxic Substances and Disease Registry) database. Statistical analysis methods such as linear regression explored associations between the SVI scores and CT scanner ages. Additionally, CT phantom image data were analyzed for image quality metrics such as noise magnitude and compared as a function of scanner technology age.

Results: Approximately 30,000 CT scanners, aged 3–28 years, and corresponding SVI scores were analyzed. Significant associations found between the CT scanner age and SVI scores ($p<0.05$), suggesting that a county’s social conditions may impact CT technology access. Data shows positive correlation between the counties with higher percentiles of persons with disabilities (slope = 0.45 yr/SVI unit, 95% CI [0.3,0.6]), those 65 or older (slope = 0.35 yr/SVI unit, 95% CI [0.2,0.5]), or in extreme poverty (slope = 0.16 yr/SVI unit, 95% CI [0.1,0.3]), and the age of CT scanners. Conversely, negative correlation was found between the counties with higher percentiles of minority populations (slope = -0.41 yr/SVI unit, 95% CI [-0.5,-0.3]), crowding (slope = -0.26 yr/SVI unit, 95% CI [-0.4,-0.1]), or cost-burdened housing (slope = -0.30 yr/SVI unit, 95% CI [-0.4,-0.2]), and the age of CT scanners. Further, analysis of comparable phantom images from scanners developed 11 and 23 years ago demonstrated an 8.7 HU increase in noise magnitude in older models.

Conclusion: The study highlights disparities in medical imaging technology across the U.S. as it relates to social vulnerability, potentially exacerbating healthcare inequities for socially vulnerable populations. The findings provide a quantitative benchmark to target future improvements and depict, for the first time, the “cost” of such disparities in terms of patient safety and image quality.

Clinical Impact: Identification of disparities in access to medical imaging technologies based on social vulnerability underscores the need for mitigating healthcare inequities to ensure equitable, patient-centered care across diverse populations. Addressing these disparities can enhance diagnostic accuracy and safety, particularly for vulnerable groups.

Montero, I. “Modeling the Radiology Department: A Digital Twin Approach”

First Author: Isabel Montero, MS
Mentor: Ehsan Samei, PhD
Training Level: PhD Student
Location: G16

Background: Clinical radiology involves a complex series of stochastic processes— patients with diverse characteristics, are referred for various imaging indications, and are scanned on equipment with differing performance and protocols. Currently there is no simulation framework applicable to these processes holistically– current tools tend to focus either on physics-based modeling of image formation, without capturing variability of clinical practice, or on workflow modeling without encompassing imaging performance.

Objective: This project aims to develop a digital twin of the radiology department that models the probabilistic movement of patients through the imaging pipeline—from referral to image interpretation—using a Monte Carlo–based framework. By integrating clinical data, imaging performance metrics, and diverse patient cohorts, the model can be used to ascertain how variability in decision-making, scanner performance, and operational workflow may collectively influence diagnostic outcomes and consistency of care.

Methods: Through interviews with key radiology personnel, a modular Python-based framework was developed to represent key stages of the imaging pipeline. Virtual cohorts are probabilistically scattered through the radiology workflow— referral, verification, scheduling, protocoling, acquisition, and interpretation. Each stage incorporates rule-based or empirically derived transition probabilities from Duke Health System data, reflecting real-world variability, such as scanner capabilities and protocoling practices. The model uses the Monte Carlo methodology to assign empirically-informed cross-sectional values for probabilities across the workflow, and how the statistics propagate across the system to affect diagnostic quality and throughput.

Results: The resulting digital twin functions as a modular simulation tool modeling variability across radiology workflow components. Each module can be independently modified, substituted, or calibrated, enabling scenario testing and system-level experimentation.

Conclusion: This study introduces a modular digital twin of the radiology workflow integrating both operational and technical aspects of medical imaging. By representing the radiology department as a probabilistic system, the framework captures how variability emerges and interacts across the clinical imaging pipeline. The tool serves as a preliminary foundation for studying and visualizing how systemic factors influence diagnostic quality and consistency.

Clinical Impact: The digital twin provides a computational environment for testing workflow and technology decisions before clinical implementation and can serve as a preliminary foundation for studying and visualizing how systemic factors influence diagnostic quality and consistency.

Mosley, I. “Assessing Motion Artifacts in Ultra-High Resolution CT for Pancreatic Cancer Imaging”

First Author: Iman Ajani Mosley
Mentor: Ehsan Samei, PhD
Training Level: Medical Student
Location: M5

Background: Accurate staging of pancreatic cancer relies on precise imaging of tumor-vessel relationships to determine surgical resectability. Ultra-high-resolution CT (UHRCT) provides finer spatial detail than conventional CT but is inherently more susceptible to physiologic motion. Among these motion sources, cardiac-induced motion has received relatively little attention. Holmes et al. provided initial evidence that cardiac motion causes measurable pancreatic displacement (0.24-1.59 mm) and significantly degrades UHRCT image quality, but comprehensive evaluation of its impact on clinical staging accuracy is limited.

Objectives: My project aims to determine how physiologic motion- particularly cardiac motion- affects UHRCT image quality and the accuracy of pancreatic cancer staging. My hypothesis is that cardiac motion introduces interpretive uncertainty, potentially leading to differences in how tumors and vessels are characterized and, consequently, how patients are managed.

Methods: Patient-specific anatomy from confirmed borderline resectable pancreatic ductal adenocarcinoma cases was integrated into XCAT anatomical phantoms that incorporate physiologic cardiac motion patterns derived from Holmes et al. The phantoms were then imaged in DukeSim, a CT scanner simulation platform, allowing direct comparison between static and motion-affected UHRCT acquisitions under identical imaging conditions.

Analysis/Results: The analysis follows a three-stage framework. The first stage focuses on subjective evaluation, in which radiologists will qualitatively assess whether motion alters visual confidence or tumor-vessel classification. Once subjective differences are established, the second stage will quantify the observed image degradation to derive objective metrics and produce a measurable figure of image degradation. The third stage will extend this framework to larger clinical datasets to evaluate how often and to what extent motion influences staging outcomes across broader patient populations. Preliminary data suggests that cardiac motion can introduce perceptible blurring in UHRCT, potentially affecting interpretive certainty.

Conclusion: Cardiac-induced motion represents an underrecognized and potentially clinically meaningful source of uncertainty in pancreatic UHRCT. Such motion may blur critical interfaces and alter the perceived resectability of borderline cases.

Clinical Impact: In borderline resectable disease, imaging determines whether patients proceed directly to surgery or require neoadjuvant therapy. Improved motion compensation in UHRCT could allow certain cases to be reclassified from borderline resectable to resectable, expanding surgical options and improving outcomes.

Murphy, D. “Lymphocytic Feature Characterization Using a Deep Learning Algorithm on Post-Radiation Lymph Nodes”

First Author: Daniel Murphy, MS
Mentor: Kyle J. Lafata, PhD
Training Level: Medical Physics Graduate Program
Location: G17

Background:
The lymph node (LN) plays a critical role as the primary site of immunogenic response in head and neck cancers and is a key determinant of cancer progression and patient outcomes. A deeper understanding of the pathological differences between involved and non-involved LN could inform strategies to optimize RT.

Objective: To evaluate the ability of a deep learning model to identify pathomic features in lymph nodes of preclinical head and neck squamous cell carcinoma (HNSCC) models as surrogates for predicting radiation therapy response.

Methods: A deep learning algorithm was tested on mice induced to express two oral cavity tumor models: immunologic human papillomavirus (HPV)-negative MOC1 tumors or poorly immunologic HPV-negative MOC2 tumors, receiving chemoradiation therapy: cisplatin (5 mg/kg, intraperitoneal) and 8 Gy irradiations on days 0 and 7. Mice survival was continuously monitored and later assessed via Kaplan-Meier survival curves. Hematoxylin & Eosin-stained whole slide images were prepared for LN specimens. For each whole slide image, ten square ROIs were selected using QuPath software with each ROI covering 1% of the total LN area. The ROIs were processed through the deep learning algorithm to detect lymphocytes. Sixteen topological features characterizing lymphocyte distribution were extracted from the pipeline. Excluding outliers, each feature value was averaged across ROIs and normalized to z-scores. Independent t-tests were conducted on each feature to identify features differentiating MOC1 and MOC2 groups.

Results: Significant differences ($p<0.05$) were found between MOC1 and MOC2 groups in nine pathomic features, including cluster score, average distance, diameter, average degree, number of nodes, mean K-core, number of K-core, average betweenness, and central node dominance. Kaplan-Meier survival analysis confirmed significantly ($p<0.05$) higher survival in the MOC1 group compared to MOC2, suggesting the feasibility of utilizing these pathologic features, identified by the deep learning pipeline, on predicting treatment outcomes.

Conclusion: The deep learning pipeline identified nine pathomic features that capture differences in immunological phenotypes of lymph nodes in pre-clinical mice models, demonstrating positive associations with survival rates.

Clinical Impact: This controlled approach enables us to evaluate the immunological landscape of LNs to potentially predict treatment response following RT and improve clinical outcomes.

Nadkarni, R. “A Virtual Preclinical Photon-Counting CT Framework for Truth-Based Imaging Optimization in Cancer Studies”

First Author: Rohan Nadkarni
Mentor: Cristian Tudorel Badea, PhD
Training Level: PhD Student
Location: G18

Background: Photon-counting detectors (PCDs) enable multi-energy CT imaging with multiple contrast agents, supporting imaging for preclinical cancer studies that use mice with head and neck squamous cell carcinoma (HNSCC). Optimizing photon-counting CT (PCCT) parameters to accurately characterize tumors is challenging in live mice due to radiation dose constraints and absence of truth-based validation that would require invasive or destructive imaging endpoints.

Objective: To enable imaging parameter optimization for preclinical cancer studies, we developed a digital phantom of a mouse with HNSCC and integrated it into our PCCT simulation that achieves high quantitative similarity to real imaging. To our knowledge, this is the first pipeline incorporating a digital mouse phantom with realistic HNSCC and validation of PCCT simulation through imaging of 3D-printed phantoms.

Methods: We transferred vasculature from a 20 micron resolution contrast-enhanced micro-CT scan of a mouse to the digital mouse whole body (MOBY) phantom using affine warps. MOBY was further enhanced by attaching a realistic HNSCC tumor synthesized by our denoising diffusion probabilistic model (DDPM). These MOBY material maps were passed into our MATLAB simulation to generate PCCT projections and reconstructions, with settings matching our real PCCT system. A multi-layer perceptron (MLP) trained on matched pairs of real and simulated 3D-printed phantoms with known material concentrations was applied for final adjustment of simulated PCCT images. Using true material maps for our MOBY phantom, we quantified how PCCT simulation affects the accuracy of iodine and barium in the tumor.

Results: Our DDPM generates tumors with realistic iodine and barium nanoparticle concentrations under both low and high barium conditions. On a 3D-printed phantom validation set, our MLP enabled accurate material decomposition of a simulated reconstruction using a sensitivity matrix measured from a real PCCT image. Material decomposition from PCCT simulation of MOBY with HNSCC showed slight overestimation of iodine and underestimation of barium within the tumor relative to the truth.

Conclusions: We established and validated a virtual preclinical PCCT pipeline integrating realistic digital mouse phantoms with DDPM generated HNSCC tumors and MLP-based calibration to real PCCT data. This framework enables accurate, low-dose optimization of multi-contrast imaging for preclinical cancer therapy studies.

Nam, J. “Association of CT-Based Body Composition and Lipoprotein(a)”

First Author: Jiung Nam
Mentor: Kirti Magudia, MD, PhD
Training Level: Medical Student
Location: M6

Background: Lipoprotein (a) [Lp(a)] is a low-density lipoprotein associated with increased risk of cardiovascular disease (CVD). Body composition (BC), the proportion of fat and muscle in the body, is also associated with CVD risk. While previous studies have shown that body mass index (BMI) synergistically predicts CVD risk with LP(a), the correlation between BC and Lp(a) has only been studied in small patient cohorts.
A fully automated deep learning workflow has recently been validated to quantify BC from CT scans with equivalency to expert manual segmentation, allowing direct BC measurement in much larger cohorts than previously possible.

Objective: To evaluate associations between Lp(a) levels and CT-derived BC metrics in a large, diverse patient cohort.

Methods: This retrospective study included all patients at Duke University from 2014 to 2024 who underwent both abdominal CT and Lp(a) testing. Deep learning analysis quantified skeletal muscle, subcutaneous fat, and visceral fat cross-sectional areas at the L3 vertebral level. Lp(a) was categorized by the clinically significant cutoff of <75 nmol/L or ≥75 nmol/L. Chi-squared, T-, and Mann–Whitney U-tests as well as linear regression were applied as appropriate.

Results: The cohort included 848 patients with median Lp(a) 53.8 nmol/L. Visceral fat area was significantly lower among patients with Lp(a) ≥75 nmol/L. Lp(a) was weakly negatively correlated with visceral fat ($r = -0.07$, $p = 0.02$). This persisted after adjusting for other BC measures and BMI ($r = -0.13$, $p = 0.001$) but not after adjusting for age, sex, race, smoking status, hypertension, diabetes, and hyperlipidemia ($r = -0.05$, $p = 0.27$). Additionally, elevated Lp(a) was more frequent among women and Black patients and was associated with higher rates of hypertension, diabetes, and hyperlipidemia.

Conclusion: Higher Lp(a) levels were modestly associated with lower visceral fat area, though this did not persist after adjusting for demographic and other clinical factors.

Clinical Impact: Automated CT-based analysis enables efficient population-level assessment of the correlation between BC and LP(a). The observed moderate association between Lp(a) and visceral fat motivates future exploration of whether LP(a) and visceral fat are independently associated with CVD.

Nasthas, A. "Bridging Anatomy and Radiology: The Educational Impact of CT Interpretation during Gross Anatomy in the First Year Medical School Curriculum"

First Author: Angelina Nasthas
Mentor: Eun Langman, MD
Training Level: Medical Student
Location: M7

Background: Integration of radiology into the pre-clinical medical school curriculum is increasingly common and can provide clinical context to basic science concepts. At our institution, cadaver computed tomography (CT) scans are acquired prior to anatomic dissection, and student anatomy groups have been provided a formal interpretation written by a radiologist. This study investigates a new teaching curriculum integrating CT interpretation skills in the first year of medical school. Students were provided instruction to prospectively interpret their cadaver's CT findings and dedicated consultation time with a radiologist to review the results.

Objective: To evaluate whether a new curriculum teaching fundamental image-interpretation skills with active interpretation of cadaver CT scans is an effective tool to teach clinical radiology to first year medical students.

Methods: A total of 117/122 (95.9%) first-year medical students completed a baseline questionnaire prior to the start of the curriculum, and 56/122 (45.9%) fully completed a follow-up survey at its conclusion. The responses were graded on a 7-point Likert scale. Identical questions on both questionnaires assessed student perceptions of the following: the role of radiologists in patient care, the process of medical image interpretation, the value of radiology knowledge, and interest in radiology as a future career path. The follow-up survey assessed student perceptions of the educational benefits of the curriculum, effects on learner engagement, and overall impressions of diagnostic radiology.

Results: After participating in prospective cadaver CT interpretation, students reported significant increases in their perception of radiologists play a key role in clinical diagnosis of disease ($p = 0.049$), perceived value that radiologists add to patient care ($p = 0.023$), view of medical image interpretation as intellectually stimulating ($p = 0.004$), and appreciation for radiology as consultants ($p = 0.008$). 50/56(89.3%) respondents agreed or strongly agreed that that they had increased understanding of human anatomy, 49/56(87.5%) that the exercise was beneficial, and 52/56(92.9%) that all medical students would benefit from the curriculum.

Conclusion: Incorporating prospective cadaver CT interpretation into gross anatomy enhances medical students' understanding and perception of radiology while enriching their anatomy learning experience. These findings support integrating radiology-led imaging sessions into preclinical anatomy curricula to foster earlier and more meaningful exposure to medical imaging and radiology.

Perkons, N. “EPIC Workflow Changes to Improve Interventional Radiology Consult Triage and Reduce Overnight Paging Volume”

First Author: Nick Perkons, MD
Mentor: Charles Kim, MD
Training Level: Resident
Location: T1

Background: While Interventional Radiology (IR) procedures for hospitalized patients have often been ordered directly by referrers, increasing patient and procedure complexity have driven a shift towards consultation whereby the IR service directly determines a plan and/or procedure based upon clinical history.

Objective: In May 2024, we converted to a consult-driven workflow with an IR consult order that collects triage information, including order priority, to populate a worklist to improve the workflow of both IR clinicians and their referrers. Only STAT priority consults generate a direct page to the on-call physician. This replaced a prior workflow wherein all procedure requests, regardless of priority, were accompanied by a page. In this study, we quantify the impact of our intervention, particularly with respect to after-hours requests.

Methods: Retrospective review identified 6,488 IR consult orders from 7/1/2024-6/30/2025. Pertinent patient and referral details were used to analyze rates of consult placement and cancellation according to priority and time. Data were analyzed using R; t-tests were used to compare continuous variables.

Results: Of 6,488 consults placed, 4,667 (71.9%) were completed while the remainder were cancelled prior to fulfillment, primarily due to either a change in clinical plan or a mistake requiring order modification. During this period 3,791 IR procedures were performed on hospitalized patients. Order priority prevented 1,452 requests from generating an unnecessary page after-hours (27.9 per week), representing 71.7% of after-hours orders. Routine requests occurred more frequently during business hours (1.08 vs. 0.138 consults/hr; $p<0.0001$), whereas no significant difference was observed for STAT consults (0.083 vs. 0.073 consults/hr; $p=0.14$). A substantial number of consults (13%, n=613) reflected requests intended for a different procedural subspecialty, including within Radiology.

Conclusions and Clinical Impact: Among other important benefits, implementation of an IR consult-driven workflow significantly reduced after-hours pages to the on-call physician by routing non-STAT consults to a routine queue. The frequency of consults ordered with STAT priority did not vary significantly with time-of-day, suggesting appropriate use of the priority modifier. A substantial incidence of erroneous consults intended for other procedural subspecialties suggests that a unified imaging-guided procedure order may further improve IR triage and referrer experience.

Perkons, N. “Retrospective Review of Outcomes Following Apheresis Port Placement”

First Author: Nick Perkons, MD
Mentor: Charles Kim, MD
Training Level: Resident
Location: T2

Background: Long-term apheresis has traditionally been accomplished with tunneled large bore catheters due to the required high flow rates. Apheresis ports, approved in 2017, provide an implantable solution capable of supporting flow rates sufficient for apheresis but with very limited published data on clinical outcomes.

Objective: The purpose of this study was to evaluate outcomes after apheresis port placement in a large cohort.

Methods: Retrospective review identified 217 apheresis ports (Powerflow, B.D., Tempe, AZ) placed in 136 patients between 09/2017 and 12/2024. Port infection was defined as port removal for the indication of infection. Port dysfunction was defined as catheter interrogation due to inability to aspirate. Chi-square testing was performed for comparison of categorical variables and cox proportional hazard models were used for time-to-event analyses.

Results: The most common indications for placement were sickle cell disease (44.2%), graft versus host disease (19.4%) and transplant rejection (18.9%). There were 0.44 initial port dysfunctions per 1000 catheter days with a substantial proportion not requiring intervention upon interrogation; there were 0.24 initial port interventions per 1000 catheter days. There were 0.18 port infections requiring removal per 1000 catheter days.

Conclusions and Clinical Impact: This study reveals that implantable apheresis ports demonstrate excellent long-term performance with very low infection and dysfunction rates that are substantially lower than historical rates for tunneled catheters and which are on par with traditional subcutaneous ports. A substantial proportion of referrals for dysfunction may be due to access error rather than intrinsic abnormality.

Reed, B. “Difference in Image Quality between Natively Reconstructed and PACS Reformatted CT Images”

First Author: Beth Reed, MS
Mentor: Justin Solomon, PhD
Training Level: Medical Physics Resident
Location: G19

Objective: The objective of this study was to compare image quality between CT images of variable slice thickness reconstructed directly at the scanner verses reformatted at a PACS workstation.

Background: CT exams may contain large, reconstructed image series that increase file size with each reconstruction. PACS workstation tools have the potential to produce read-time reformats that could replace native reconstructions, thereby reducing resource-intensive workflow and time requirements as well as simplifying protocol management. Differences in image quality between native and read-time reconstructions are unknown.

Methods: The American College of Radiology (ACR) CT image quality phantom (Gammex 464) was imaged using the institution’s lung cancer screening protocol on two CT systems (GE Discovery CT750 HD, Siemens SOMATOM Definition Flash). Images were reconstructed at varying slice thicknesses (0.6-7mm). The thinnest axial series from each system were sent to a PACS workstation (Visage 7.0) and reformatted to matching slice thicknesses. Measurements - including noise power spectrum (NPS), contrast, and task transfer function (TTF) - were made using TG233 methodology with a standard publicly available software tool (IMQUEST) and compared between “native” (i.e. from scanner) vs PACS reconstructed images.

Results: Noise from native images was higher compared to PACS images by 21% on average for the GE scanner. Noise was comparable between native and PACS images for the Siemens scanner (< 6% difference on average). Native image noise texture was marginally higher than PACS images (< 11.5% difference on average). Contrast was comparable between native and PACS images (<8% difference on average). Spatial resolution was marginally improved on native images compared to PACS images (< 7% difference on average).

Conclusion: PACS reformatted images demonstrated only a marginal difference from native reconstructed images in image quality properties of noise, noise texture, contrast, and spatial resolution.

Clinical Impact: This project supports the ability to substitute selected native reconstructions with PACS reformats. This substitution would streamline the management of CT protocols and current resource-intensive workflows.

Riley, B. “A Patient-Specific Digital Twin Framework to Model Spatial Immune Dynamics in Head and Neck Squamous Cell Carcinoma”

First Author: Breylon Akeli Riley
Mentor: Kyle J. Lafata, PhD
Training Level: Medical Physics Graduate Program
Location: G20

Background: The spatial architecture of the tumor microenvironment (TME) is a critical, yet poorly modeled, determinant of immunotherapy response in head and neck squamous cell carcinoma (HNSCC). Static histology images fail to capture the dynamic cellular interactions that dictate clinical outcomes.

Objective: To develop and validate an applied mathematical framework for constructing patient-specific "digital twin" models of the HNSCC TME. This model will formally define how spatial rules govern immune efficacy and provide a platform for in-silico biomarker discovery.

Methods: We built a dynamical systems model parameterized from multiplex immunohistochemistry. The system state is initialized with spatial coordinates of CD45+ (immune) and PanCK+ (tumor) cells. Immune agents execute a biased random walk towards tumor cells, with exhaustion governed by first-order kinetics. Stromal boundaries are integrated from α-SMA+ measurements to constrain the system.

Results: Initial model implementations successfully recapitulate heterogeneous immune-tumor interaction patterns. Analysis of model trajectories indicates that initial spatial distribution is a stronger predictor of tumor burden than immune cell density alone. The framework quantifies how stromal geometries create "immune deserts," permitting tumor survival despite proximal immune infiltration.

Conclusion: We present a foundational mathematical framework for modeling the HNSCC TME as a dynamical system. This approach provides a rigorous platform to move beyond static correlative analysis by simulating the consequences of tissue topology.

Clinical Impact: This model establishes a novel radiopathomic platform for predicting immunotherapy response. By creating patient-specific digital twins, it enables in-silico testing of treatment strategies and identifies spatial biomarkers, directly informing personalized therapeutic decisions for HNSCC patients.

Stevens, J. "A stochastic modeling framework to integrate radiomic feature representations: development and proof of concept application to PET/CT images of oropharyngeal cancer"

First Author: Jack B Stevens
Mentor: Kyle J. Lafata, PhD
Training Level: PhD Student
Location: G21

Background: Radiomic analyses (i.e., high-throughput computational algorithms that extract quantitative features from medical images) typically separate measurements of tumor texture and morphology, despite their intrinsic interdependence. The degree to which these properties should be studied independently remains unclear.

Purpose: To develop a mathematical framework that unifies texture and morphology into a topological representation of tumors, and to compare its feature representation with common image-based measures of texture and morphology in PET/CT images of patients undergoing definitive chemoradiation therapy for oropharyngeal cancer (OPC).

Methods: Primary tumors were stochastically sampled using Langevin dynamics. The potential function required for this process was derived directly from PET/CT imaging data using quantum clustering. Solving for the potential captured textural information across imaging modalities. Langevin trajectories were then used to probe the tumor's topological landscape. Mean exit times of Langevin trajectories generated a tumor-specific topological map intrinsically combining texture and morphology. Statistical features extracted from these maps defined a patient-specific feature space. The algorithm was numerically validated against analytical solutions for a uniform sphere, then applied as proof-of-concept to 56 OPC patients enrolled on a prospective trial evaluating early response to 20 Gy ± concurrent chemotherapy. Extracted topological features were compared with standard PET radiomics via cluster analysis and correlation matrices.

Results: The algorithm showed strong agreement with analytical solutions (mean-absolute-error = 0.014). Distributions of mean exit times represented patient-specific tumor topology. Cluster analysis revealed that topological features provide information distinct from traditional PET radiomics, which was confirmed by variability in feature correlation between the two methods.

Conclusion: Our approach integrated different aspects of the tumor phenotype into a singular measure of tumor topology. Preliminary findings suggest that topological features provide complementary information to standard radiomics, highlighting the future potential for this technique as a prognostic biomarker for early treatment response in patients with OPC.

Tan, R. “Investigating Intra-tumoral Heterogeneity Driven by Nutrient Dynamics Using an In-silico Avascular Tumour Growth Model”

First Author: Runhe Tan
Mentor: Kyle J. Lafata, PhD
Training Level: Medical Physics Graduate Program
Location: G22

Background: Avascular tumour growth exhibits a proliferating rim (P), a quiescent band (Q), and a necrotic core (N) governed by nutrient availability and contact-inhibited cell motion. The Sherratt–Chaplain framework captures these dynamics via contact-inhibition fluxes and nutrient-dependent transitions among P, Q, and N.

Objective: To develop a modular pipeline that (i) generates image-like cell-state maps from a dynamic nutrient model and (ii) quantifies how the nutrient consumption/uptake parameter, α, affects intra-tumoral heterogeneity and radiomic features.

Methods: We implemented a Chaplain–Sherratt 1D partial-differential-equation model of avascular tumor growth under dynamic nutrient conditions with explicit time stepping and zero-flux boundaries. The solver outputs radial cell-state densities p, q, n over time. A Monte-Carlo module samples shells and assigns cell types by cumulative probabilities [p, q, n], placing points inside a 2D circular boundary. We used a manual voxelization routine to convert cell coordinates to voxel maps of each cell type. We normalized intensities across α and time and generated masks by radially segmenting the total-cell image. The voxel maps of different cell channels then yield normalized Shannon entropy maps ($H \in [0,1]$). The tool was then used to extracted intensity masks for downstream radiomic analyses.

Results: Across $\alpha = \{0.1, 0.3, 0.5, 0.7, 1.0\}$, higher α (stronger nutrient consumption) lowered nutrient level, narrowed the proliferative rim, and expanded Q/N earlier, which leads to lower texture heterogeneity and earlier saturation of necrosis. Joint entropy trajectories reach maximum during expansion followed by stabilization. The maximum timing and magnitude shifted systematically with α. Masks remained stable across time, enabling consistent feature computation.

Conclusion: This in-silico tumor model mechanistically links a dynamic nutrient field to intra-tumoral heterogeneity and radiomic features. It enables controlled, reproducible computational experiments that study the effects of nutrient dynamics on image heterogeneity.

Clinical Impact: By linking biophysical parameters to image features, this tool can generate digital phantoms for radiomics QA, sensitivity analyses, and hypothesis testing. It can also support study design and biomarker strategies that reflect underlying tumour biology.

Zaveri, S. “Scan-Rescan Repeatability of Hippocampal Volume Measurements in Patients with Low-grade Glioma: Comparison of Automated Software Packages”

First Author: Suraj Zaveri
Mentor: Daniel Barboriak, MD
Training Level: Medical Student
Location: M8

Background: Neurocognitive impairment is a leading cause of reduced quality of life in patients with brain tumors and is particularly common after radiation therapy, affecting over 90% of long-term survivors following whole-brain radiotherapy (WBRT)1. In patients with low-grade glioma (LGG), cognitive deficits remain prevalent even among long-term survivors without disease progression2. While patient-reported outcomes studies assess psychosocial impact directly, validated imaging biomarkers would be useful to define the anatomic basis of unsuccessful survivorship. Hippocampal volume (HV) is a sensitive marker of cognitive decline in aging and neurodegenerative disease. Reduced HV predicts conversion to mild cognitive impairment or Alzheimer’s disease3,4. The hippocampus is particularly radiosensitive, with radiation causing dose-dependent decreased neurogenesis and atrophy5. Hippocampal-sparing WBRT has been shown to mitigate cognitive decline6. Before HV can serve as a biomarker in LGG, its reproducibility across MRI-based segmentation platforms must be established.

Objective: To evaluate short-term reproducibility of automated hippocampal and normalized hippocampal volume measurements across multiple MRI software platforms in patients with low-grade glioma.

Methods: Scan-rescan repeat high-resolution three-dimensional (3D) T1-weighted magnetic resonance (MR) images from 26 adults with World Health Organization (WHO) grade II LGG were acquired at both baseline and six months. Hippocampal volumes were quantified using automated software packages NeuroQuant, FSL/FIRST, HippoSeg, and FreeSurfer. Reproducibility-related metrics including repeatability coefficients, intraclass correlation coefficients, and concordance correlation coefficients derived from mixed-effects models were calculated.

Results: Hippocampal measurements demonstrated excellent scan–rescan reliability for NeuroQuant and FSL/FIRST (intraclass correlation coefficient >0.90), moderate reliability for HippoSeg (0.75–0.90), and variable performance for FreeSurfer. Normalization did not improve reliability. No significant hippocampal volume change was detected over six months. Absolute HVs were highest with NeuroQuant and FSL/FIRST and lowest with FreeSurfer, though inter-software correlations remained strong ($r \geq 0.55$, $p<0.01$).

Conclusion: Automated hippocampal volumetry in LGG is highly reliable, particularly using NeuroQuant and FSL/FIRST. Normalization, laterality, scanner type, and interval length did not affect consistency, though HV measurements varied across software.

Clinical Impact: Reliable automated hippocampal quantification supports its potential as an imaging biomarker of neurocognitive outcomes in brain tumor survivorship and radiotherapy trials.